

Mixing and reaction in turbulent plumes: the limits of slow and instantaneous chemical kinetics

N. Mingotti[†] and S. S. S. Cardoso

Department of Chemical Engineering and Biotechnology
University of Cambridge, Philippa Fawcett Drive, Cambridge CB3 0AS, UK

(Received xx; revised xx; accepted xx)

We investigate the behaviour of a reactive plume in the two limiting cases of slow and instantaneous chemical reactions. New laboratory measurements show that while the slow reaction between the source and entrained chemical species takes place within the whole volume of each eddy in the plume, the fast reaction develops preferentially at the periphery of the eddies. We develop a new model that quantifies the mixing of the reactive buoyant fluids at the Batchelor scale and thereby the progress of the fast reaction. We present a series of new experimental results which suggest that a critical distance from the source, z_{crit} , exists at which the volume of fluid which is entrained from the ambient is equal to that which is mixed within the plume at the Batchelor scale. For $z > z_{\text{crit}}$, only a fraction of the entrained fluid is rapidly mixed and reacts with the plume fluid. The results of the new experiments enable us to quantify the distance from the source at which an instantaneous reaction reaches completion, and show that it can be significantly larger than the distance L_s at which the stoichiometric dilution of the plume fluid is achieved. In the limit of an instantaneous reaction, the longitudinal profiles of source chemical concentration in the plume depend on $(z_{\text{crit}}/L_s)^{5/6}$. The predictions of the model are validated against the experimental results, and the profiles of source chemical concentration in the plume for slow and fast reactions are compared.

Key words: Plume, mixing, reaction

1. Introduction

Turbulent plumes are observed in a variety of natural flows, such as the fluid columns that rise above hydrothermal vents in the deep ocean (Luption *et al.* 1985) or volcanic vents during an eruption (Woods 2010; Sparks *et al.* 1997). At a range of different scales, turbulent plumes are also encountered in industrial flows, including discharges of smoke from chimneys, effluents from submerged pollutant outlets and leaks from pipelines (Campbell & Cardoso 2010). While rising above a localised source of buoyancy, plumes entrain fluid from the surrounding ambient (Morton *et al.* 1956), leading to a progressive dilution of the source fluid. Internal processes such as chemical reaction, dissolution and phase change may also contribute to buoyancy changes in the plume.

A number of recent studies have considered the interaction of chemical reaction and the buoyant flow in turbulent plumes. Most of these have focussed on the effects of reaction

[†] Email address for correspondence: nm441@cam.ac.uk

13 on buoyancy, through a change in composition or enthalpy, and its influence on the flow
14 field. Conroy & Llewellyn Smith (2008) and Campbell & Cardoso (2010) investigated the
15 behaviour of a single-phase plume with internal buoyancy generation. Their numerical
16 and analytical studies describe the behaviour of the plume both in the region near the
17 source and in the far field, and quantify the impacts of different buoyancy fluxes produced
18 by the reaction relative to the flux at the plume source. In the context of carbon-dioxide
19 and methane releases in the ocean, Cardoso & McHugh (2010) and Domingos & Cardoso
20 (2013) considered a two-phase plume with a first-order reaction at the interface between
21 the droplets/bubbles and the plume liquid. They identified the conditions for which the
22 plume buoyancy is controlled by either the density stratification in the environment or by
23 the chemical dissolution. Woods & Caulfield (1992) noted that when a sufficiently large
24 flux of negative buoyancy is generated during the non-linear mixing of the plume and
25 ambient fluids, then the bulk density of the plume fluid may become larger than that of
26 the surrounding ambient fluid at a finite distance from the source. In this case the
27 plume gradually transitions into a collapsing fountain. Woods & Caulfield (1992; 1995)
28 explored some of the dynamics of this transition using experiments with mixtures of
29 methanol and ethylene glycol (MEG) and water, which exhibit a reversal of buoyancy as
30 the MEG mixes with water. They reported intermittent formation of collapsing fountains
31 and convective plumes in a range of experimental conditions.

32 When the chemical interaction has negligible effects on the buoyancy of the plume,
33 the dynamics of the flow are described by the classical theory (cf. Morton *et al.* 1956),
34 while the kinetics of the reaction determine the process of consumption of reactants
35 in the fluid. For example, when warm, acidic industrial discharges are released into the
36 natural environment, buoyant plumes rise through and mix with the surrounding ambient
37 fluid. Ulpre *et al.* (2013) presented the results of a series of laboratory experiments, in
38 which an acidic plume descended through a tank containing an alkaline solution. They
39 quantified the distance from the source at which the [plume fluid reaches the stoichiometric
40 dilution, and measured the longitudinal concentration of source chemical](#) in the two cases
41 of a strong acidic plume descending through either (i) a strong or (ii) a weak alkaline
42 ambient.

43 In all the above studies, it was assumed that the chemical reaction occurs on a
44 larger time scale than the small-scale mixing in the plume. Indeed, few studies have
45 considered plume flows where the reaction is limited by turbulent mixing. Komori & Ueda
46 (1984) measured the concentration of chemical species in a gaseous plume undergoing a
47 moderately fast, second-order chemical reaction and found that the turbulence effects
48 on the reaction rate are significant: in particular, they noted that the effect of the
49 concentration fluctuations on the reaction rate can be as much as 20 times larger than that
50 of the mean concentrations. Domingos & Cardoso (2015) demonstrated that turbulent
51 thermals undergoing an instantaneous chemical reaction are non-uniformly mixed and
52 quantified the delay in the completion of the reaction, compared to the classical well-
53 mixed scenario.

54 In the present study, we address this gap in knowledge by investigating the behaviour
55 of a plume with a second-order chemical reaction [that does not affect the buoyancy flux of
56 the plume](#). We present and contrast the results of a series of new laboratory experiments
57 focussing on two limiting scenarios, those of fast and slow reactions compared to the
58 mixing across the plume. We measure for the first time the size of eddies containing
59 reactant and its evolution along the plume. We show that a fast reaction occurs mainly
60 at the periphery of the turbulent eddies and we relate the local rate of chemical conversion
61 to that of mixing on the Batchelor scale. We propose a new theoretical model to predict
62 the length scale for complete reaction as a function of the small-scale mixing in the

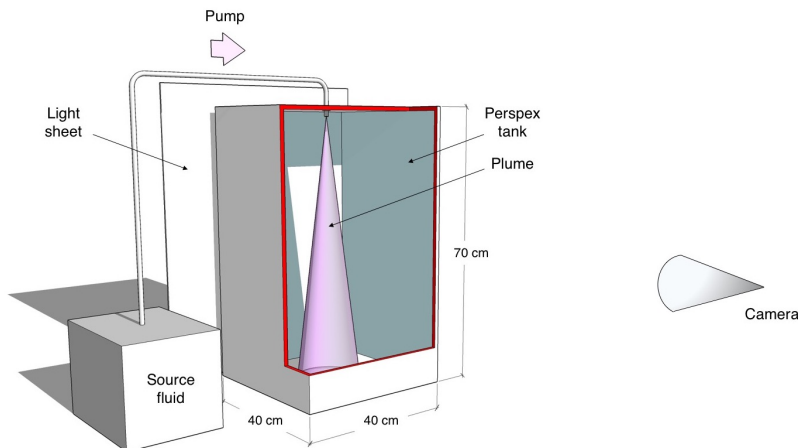


FIGURE 1. Schematic representation of the experimental setup.

63 plume. Our model is validated with the experimental results, and shows that in the
 64 limit of an instantaneous reaction, the distance from the source at which the source
 65 reactant in the plume is consumed can be significantly larger than that at which the
 66 stoichiometric dilution is achieved. This means that reactive discharges of buoyant fluid
 67 will be fully neutralised at larger distances from the source than previously reported. The
 68 experimental observations presented in the paper enable us to quantify these distances,
 69 as well as the longitudinal concentration profiles of source reactant in the plume.

70 The structure of the paper is as follows: in section 2, we describe the experiments and
 71 the technique used to process the data. In section 3, we describe the chemical reactions
 72 used in the experiments, and give details about their kinetics. In section 4, we discuss the
 73 main experimental observations and the different processes of consumption of reactants
 74 in plumes with a fast or a slow reaction. We present the new model in section 5 and draw
 75 conclusions in section 6.

76 2. Setup and calibration of experiments

77 2.1. Experimental setup

78 A series of experiments was carried out to explore the behaviour of turbulent, single-
 79 phase plumes with a chemical reaction. The experiments were run in a perspex tank
 80 of dimensions $40 \times 40 \times 70$ cm (figure 1). Before the beginning of each experiment,
 81 the tank was filled with a dilute aqueous solution of an acid. (i) Acetic, or (ii) nitric, or (iii)
 82 ascorbic acid were used to investigate the effects of different reactions (see table 1). To
 83 study the impacts of different source conditions, two round nozzles of a radius 0.6 and
 84 1.2 mm were used in the experiments. During each experiment, one of the nozzles
 85 was placed at the top of the tank and was connected to a glass beaker containing an aqueous
 86 solution of (i) ammonium hydroxide, or (ii) sodium hydroxide, or (iii) methylene blue
 87 (see table 1). To increase the density of the source fluid in the beaker relative to that of
 88 the fluid in the tank, either sodium chloride or sucrose was added to the solution (see
 89 table 1). In experiments (i) and (ii), a few drops of phenolphthalein colour indicator were
 90 added to the clear fluid in the beaker (see table 1); the addition of the indicator did not
 91 affect the density or viscosity of the fluid. Owing to the presence of methylene blue in
 92 the solution, no extra dye was added to the fluid in the beaker in experiments (iii).

93 During each experiment, the relatively dense fluid in the beaker was supplied to the

<i>Exp.</i>	<i>Ambient fluid</i>	<i>Plume fluid</i>	<i>Increase density of plume fluid</i>	<i>Dye</i>
(i)	CH ₃ COOH acetic acid	NH ₄ OH ammonium hydroxide	Sodium chloride	Phenolphthalein
(ii)	HNO ₃ nitric acid	NaOH sodium hydroxide	Sodium chloride	Phenolphthalein
(iii)	H ₂ A ascorbic acid	MB methylene blue	Sucrose	-

TABLE 1. Reactive systems used in the experiments.

94 tank using a peristaltic pump at a controlled flow rate Q_0 in the range $1 - 2 \times 10^{-6} \text{ m}^3$
 95 s^{-1} (see tables 2-4). On entering the tank, the outflow from the nozzle rapidly became
 96 turbulent (see Appendix A), and formed a dense plume which descended through the
 97 surrounding ambient fluid. The tank was backlit using a light panel of dimensions $50 \times$
 98 80 cm (manufactured by Electro-LuminX Lighting Co.) positioned at the rear of the
 99 tank (see figure 1). A Nikon D300 camera, located in front of the tank, was used to
 100 capture pictures at a frequency of 5 Hz (figure 2a). Each image had 2136 pixels in the
 101 horizontal direction and 3212 pixels in the vertical direction, resulting in a resolution
 102 0.218 mm/pixel . The experiments were performed in a dark room, and so the only light
 103 detected by the camera had passed through the fluid in the tank. Consequently, the
 104 line-of-sight average distribution of the dyed plume fluid in the tank could be inferred
 105 based on the distribution of the light attenuation in the images. In figure 2b, false colours
 106 are used to illustrate the instantaneous distribution of the dyed plume fluid 10s after the
 107 beginning of experiment 1 (see table 2). In order to ensure that the results are repeatable
 108 and reproducible, each reactive experiment was repeated up to three times. In figures
 109 3, 4, 7, 10 and 11 we show the different results obtained when repeating experiment 5;
 110 these results are labelled "5a", "5b", and "5c". For all other experiments, we plot the
 111 average of the results obtained from each run. For calibration purposes, and in order to
 112 compare the properties of a plume with chemical reaction to those of an inert plume,
 113 each reactive experiment was also repeated using fresh water as the ambient fluid in the
 114 tank. Each experiment typically lasted 2.5-3 minutes, during which approximately 750-
 115 900 photographs were captured. A time average of these photographs was calculated for
 116 each experiment to estimate the average distribution of the light attenuation produced
 117 by the plume fluid during the experiment (figure 2c).

2.2. Turbulent plumes in fresh water

118 The outcomes of the experiments with no chemical reaction were analysed first, in order
 119 to: (i) estimate the errors associated with the light attenuation experimental technique;
 120 (ii) identify the virtual origin of the plume and estimate its entrainment coefficient;
 121 and (iii) measure the time-averaged light attenuation produced by the plume fluid as it
 122 becomes increasingly diluted while descending through the tank. This will be used as a
 123 reference in section 5, in which the effects of the chemical reaction are investigated.

124 In a plume descending through an inert unstratified ambient, the buoyancy flux
 125

$$B = 2\pi \int_0^\infty \frac{\rho - \rho_a}{\rho_a} r g u dr \quad (2.1)$$

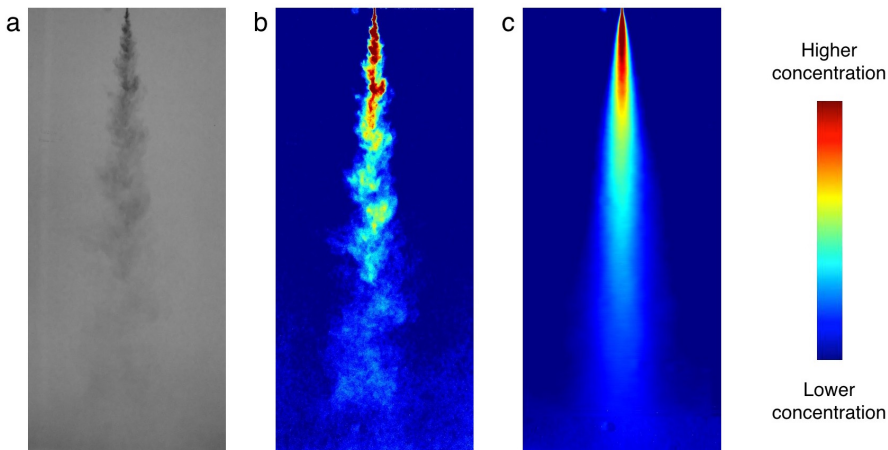


FIGURE 2. (a) Photograph of an inert plume descending through fresh water; (b) The depth-averaged distribution of light attenuation is visualised using false colours; (c) Time- and depth-averaged distribution of light attenuation. This image has been obtained by averaging 200 photographs which were captured during 40 s at the beginning of the experiment.

is conserved (Morton *et al.* 1956); here, ρ and ρ_a (kg m^{-3}) are the densities of the plume and the ambient fluids respectively, r (m) is the radial distance of a parcel of fluid from the plume centreline, g (m s^{-2}) is the gravitational acceleration, and u (m s^{-1}) is the downward speed of the plume fluid. In order to estimate the errors associated with the image analysis technique, the photographs captured during each experiment with no chemical reaction were used to quantify the flux of light attenuation at different distances from the plume source, and verify whether this flux was conserved. Figure 3 illustrates how the flux of light attenuation was measured. For each picture captured during an experiment, we measured the horizontally averaged profile of light attenuation in a rectangular region surrounding the plume (red box in figure 3a). A time series of these profiles is plotted in figure 3b: dark fronts stretching diagonally are observed in this image, illustrating the downward motion of the plume eddies over time. We used the Hough transform as available in Matlab to identify the fronts (red lines in 3b), measure their gradients, and thereby estimate the speed of the eddies at different distances below the source (cf. Mingotti & Woods 2016). We multiplied the cross-sectional light attenuation profiles by the associated speed profiles to infer the magnitude of the flux of light attenuation. Figure 3c shows that across a number of experiments the time-averaged fluxes of light attenuation were approximately conserved, with fluctuations of order 5-7%, in the region of the tank spanning between the plume source and the expected stoichiometric distance in the reactive experiments below (cf. Ulpre *et al.* 2013). This indicates that in our experiments the attenuation of the light through the tank was approximately proportional to the concentration of dye in the plume fluid in the tank.

Plume theory indicates that in the absence of any chemical reaction, the reduced gravity of the plume fluid g' and the plume radius b vary with distance from the source, z (Morton *et al.* 1956) according to

$$g'(z + z_0) = \frac{B}{Q(z + z_0)} \propto B^{\frac{2}{3}}(z + z_0)^{-\frac{5}{3}} \quad (2.2)$$

and

$$b(z + z_0) = \frac{6}{5}\alpha(z + z_0) \quad (2.3)$$

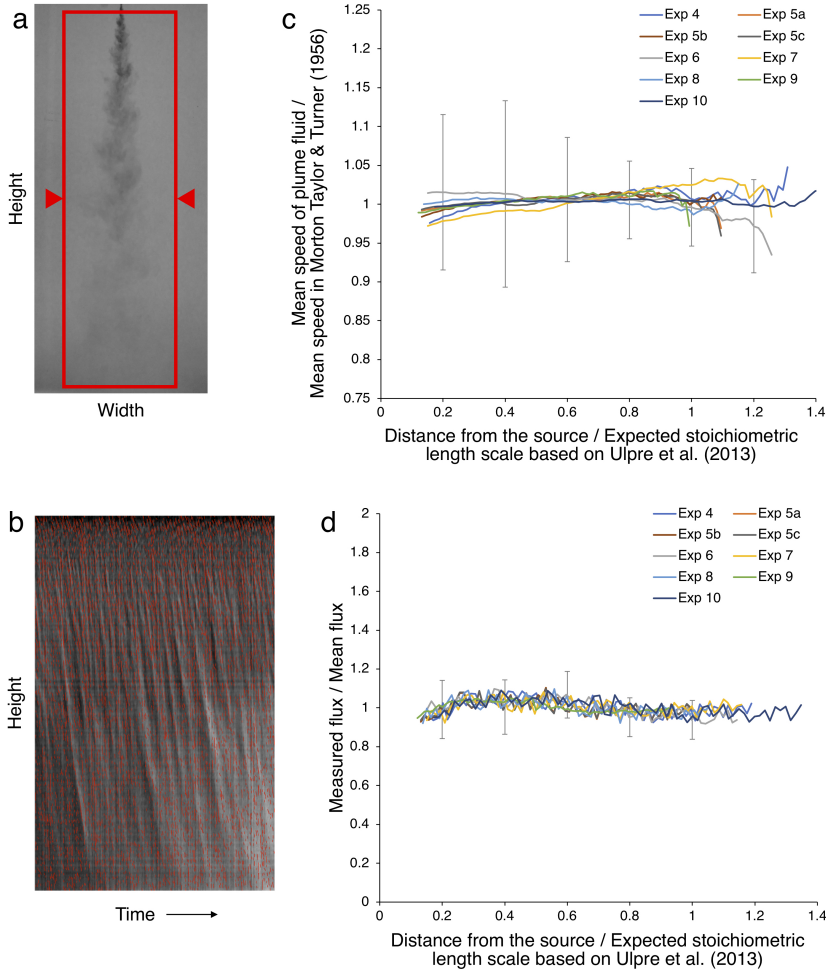


FIGURE 3. (a) For each image captured during an inert experiment, the horizontally-averaged profile of light attenuation is estimated across the width of the red box; (b) a time series of these profiles is plotted, and used to measure the characteristic speed of the descending eddies at different distances below the plume source; (c) the measured eddy velocity is compared with the top-hat speed $u = (6\alpha\pi^2/5\lambda^2)^{-2} (B/z)^{1/3}$ (Morton *et al.* 1956), error bars are plotted for experiment 6; (d) the flux of light attenuation along the plume is estimated by multiplying the measured intensity of light attenuation produced by the plume fluid at a given distance from the source by the associated measured speed. It is seen that this flux is approximately constant, with deviations of order 5-10% associated with the limitations of the image analysis technique. This indicates that light attenuation across the tank is linearly proportional to the concentration of dye in the plume fluid.

152 respectively. Here, top-hat radial profiles are assumed (cf. Morton *et al.* 1956; Papanicolau
 153 & List 1988), while z_0 (m) denotes the vertical distance between the actual source and
 154 the virtual source of the plume (Hunt & Kaye 2001) and α is the entrainment coefficient
 155 (Morton *et al.* 1956). To locate the virtual origin in our experiments, we first measured the
 156 time-averaged mean profiles of light attenuation along the plume's centreline in a number
 157 of experiments (figure 4a). Using equation 2.2 and the best fit of the results (figure 4b),
 158 we obtained $z_0 = (5.3 \pm 0.2) \times 10^{-3}$ m. For comparison, two filling box experiments were
 159 also performed in the tank using the method described by Linden *et al.* (1990), leading to

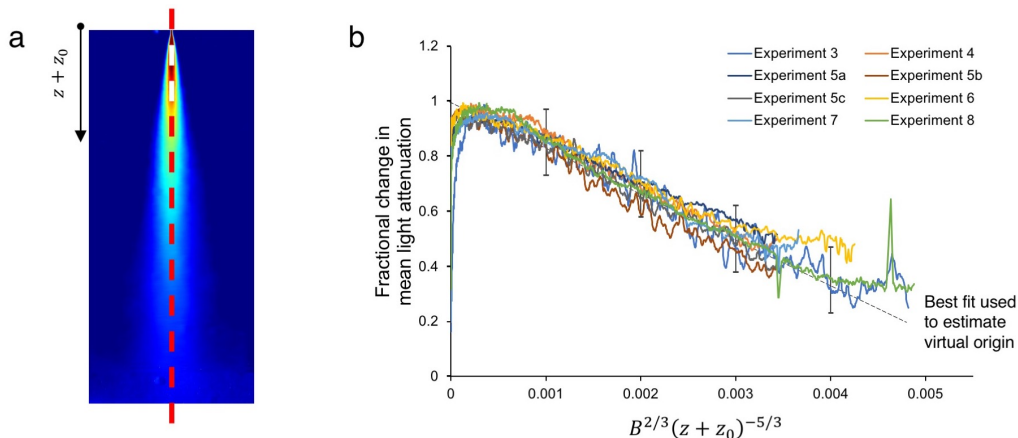


FIGURE 4. A number of time-averaged light attenuation profiles along the plume centreline are compared to estimate the virtual origin of the plume in our experimental setup.

160 a very similar result, $z_0 = (5.2 \pm 0.3) \times 10^{-3}$ m (see Appendix A). For each experiment,
 161 the time-averaged image of the flow illustrated by figure 4a was used to measure the
 162 plume radius b as a function of distance from the virtual source. At any particular height
 163 in the tank, we first measured the Gaussian width b_G between the plume vertical axis
 164 and the points at which the time-averaged dye concentration is $1/e$ of that on the axis
 165 (Morton *et al.* 1956). For conservation of mass and momentum, the top-hat radius of the
 166 plume was then defined as $b(z + z_0) = \sqrt{2}b_G(z + z_0)$. Equation 2.3 and our measurements
 167 of b were used to estimate $\alpha = 0.10 \pm 0.02$ in our experiments. Our estimates of both z_0
 168 and α are in good agreement with the literature (e.g., Bower *et al.* 2008).

169 3. Reactive systems

170 3.1. Fast reaction between acetic acid and ammonium hydroxide

171 Two sets of experiments have been carried out to explore the behaviour of plumes with
 172 a fast chemical reaction. In the first set, an aqueous solution of acetic acid was used as the
 173 ambient fluid in the tank, and a solution of ammonium hydroxide was used as the plume
 174 fluid (see tables 1 and 2). The concentrations of chemicals used in this set of experiments
 175 are listed in table 2 and discussed in appendix B. Within the range of concentrations
 176 used, the chemical reaction between acetic acid and ammonium hydroxide had negligible
 177 effects on the density of the solutions (Domingos & Cardoso 2015), and did not affect
 178 the entrainment coefficient α (see section 2.2 and appendix A). Inert sodium chloride
 179 was added to the plume fluid to increase its density relative to the ambient fluid. The
 180 products of the reaction between acetic acid and ammonium hydroxide are ammonium
 181 acetate and water



182 The rate law of this second order reaction is

$$r = k_{r_1} [\text{CH}_3\text{COOH}] [\text{NH}_4\text{OH}] \quad (3.2)$$

183 with $k_{r_1} \approx 10^{11} \text{ M}^{-1} \text{ s}^{-1}$ at 20°C (Someya *et al.* 2009). Acetic acid and ammonium
 184 hydroxide are a weak acid and a weak base respectively, and therefore they are partly
 185 dissociated in their solutions, according to the following chemical equilibria (Housecroft

186 & Constable 2002)



187 and



188 It follows that the equilibrium constant for the reaction between acetic acid and ammo-
189 nium hydroxide is given by

$$\frac{K_{\text{CH}_3\text{COOH}} \times K_{\text{NH}_3}}{K_w} = 3.2 \times 10^4 \quad (3.5)$$

190 in which K_w (M^2) is the dissociation constant for ionised water,

$$K_w = [\text{OH}^-] [\text{H}^+] = 10^{-14} \quad (3.6)$$

191 Since the constant given by equation 3.5 is large, the reaction is product-favoured and
192 driven practically to completion (Housecroft & Constable 2002).

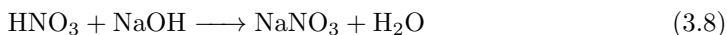
193 To observe the motion of the plume fluid in the tank and track the progress of
194 the reaction, a few drops of phenolphthalein indicator were added to the solution of
195 ammonium hydroxide and sodium chloride just before the beginning of each experiment.
196 Phenolphthalein is a weak acid, which reacts according to the following equilibrium
197 (Housecroft & Constable 2002)



198 In equation 3.7, HInd is the colourless acidic form of phenolphthalein, while Ind^- is
199 the conjugate basic form, which is characterised by a pink/purple colour (Domingos
200 & Cardoso 2015). Hence, an alkaline solution containing phenolphthalein is coloured;
201 however the colour fades when the pH of the solution decreases beyond neutralisation
202 (Wittke 1983). The relationship between colour intensity and depletion of chemical is
203 linear (Domingos & Cardoso 2015).

204 3.2. Fast reaction between nitric acid and sodium hydroxide

205 In the second set of experiments involving a fast reaction between the plume and
206 the ambient fluid, a solution of nitric acid was used as the ambient fluid in the tank,
207 and a solution of sodium hydroxide was used as the plume fluid (see tables 1 and 3).
208 Within the range of concentrations used, the chemical reaction between nitric acid and
209 sodium hydroxide did not affect the density of the solutions (Ulpre *et al.* 2013), nor the
210 entrainment coefficient α (see section 2.2 and appendix A). Just as in the first set of
211 experiments, inert sodium chloride and a few drops of phenolphthalein indicator were
212 added to the solution to control its density and colour. The products of the reaction are
213 sodium nitrate and water (Ulpre *et al.* 2013)



214 Nitric acid and sodium hydroxide are a strong acid and a strong base respectively, and
215 therefore we expect them to be completely dissociated in their solutions. The reaction
216 given in equation 3.8 is instantaneous (Atkins 1978).

217 3.3. Slower reaction between ascorbic acid and methylene blue

218 A third set of experiments was carried out to observe the behaviour of plumes with
219 a slower chemical reaction. In these experiments, a solution of methylene blue was used
220 as the plume fluid, while a solution of ascorbic acid was used as the ambient fluid in

<i>Exp.</i>	Q_0 ($\times 10^{-6}$)	r_0 ($\times 10^{-3}$)	ρ_b^0/ρ_a	B ($\times 10^{-6}$)	Γ_0 ($\times 10^{-2}$)	L_{M_0}	C_a ($\times 10^{-3}$)	C_b^0 ($\times 10^{-1}$)	D_s	L_s
1	2.0	1.2	1.074	1.45	2.78	0.024	2.979	3.844	129.0	0.380
2	2.0	1.2	1.074	1.45	2.78	0.024	3.426	3.844	112.2	0.349
3	2.0	1.2	1.074	1.45	2.78	0.024	3.873	3.844	99.2	0.325
4	2.0	1.2	1.074	1.45	2.78	0.024	4.469	3.844	86.0	0.298
5	2.0	1.2	1.074	1.45	2.78	0.024	2.979	2.329	78.2	0.282
6	2.0	1.2	1.074	1.45	2.78	0.024	5.959	3.844	64.5	0.252
7	2.0	1.2	1.074	1.45	2.78	0.024	2.979	1.560	52.4	0.223
8	2.0	1.2	1.074	1.45	2.78	0.024	4.022	1.560	38.8	0.187
9	2.0	1.2	1.074	1.45	2.78	0.024	5.959	1.560	26.2	0.149
10	2.0	1.2	1.074	1.45	2.78	0.024	5.214	0.784	15.0	0.108
11	2.0	1.2	1.148	2.90	5.56	0.017	4.469	3.844	86.0	0.260
12	2.0	1.2	1.037	0.73	1.39	0.034	4.469	3.844	86.0	0.343

TABLE 2. Conditions for experiments (i): ammonium hydroxide and acetic acid (see section 3.1). We let Q_0 ($\text{m}^3 \text{s}^{-1}$) denote the source volume flux, r_0 (m) the radius of the nozzle, ρ_b^0/ρ_a the ratio between the density of the plume fluid at the source and that of the ambient fluid, B ($\text{m}^4 \text{s}^{-3}$) the buoyancy flux. Γ_0 is the Morton number at the source (see Appendix A), while L_{M_0} (m) is the length scale for the near-source region in which the flow is affected by the supplied momentum flux (see Appendix A). C_a (M) is the concentration of acetic acid in the ambient fluid, C_b^0 (M) is the concentration of ammonium hydroxide in the plume fluid at the source, D_s is the stoichiometric dilution coefficient given by equation 5.12, L_s (m) is the stoichiometric length scale given by equation 5.13. In our calculations, we use $\nu = 1.0 \times 10^{-6}$ ($\text{m}^2 \text{s}^{-1}$) as the kinematic viscosity of water at 20°C (Atkins 1978). In all experiments, the Reynolds number at the source is $Re_0 = 1061$, the Schmidt number associated with the plume fluid is $Sc_b = 502$ (Perry & Green 2008), and that associated with the ambient fluid is $Sc_a = 829$ (Vitagliano & Lyons 1956).

<i>Exp.</i>	Q_0 ($\times 10^{-6}$)	r_0 ($\times 10^{-3}$)	ρ_b^0/ρ_a	B ($\times 10^{-6}$)	Γ_0 ($\times 10^{-2}$)	L_{M_0}	C_a ($\times 10^{-3}$)	C_b^0 ($\times 10^{-1}$)	D_s	L_s
13	2.0	1.2	1.074	1.45	2.78	0.024	0.343	0.384	112.2	0.349
14	2.0	1.2	1.074	1.45	2.78	0.024	0.298	0.233	78.2	0.282
15	2.0	1.2	1.074	1.45	2.78	0.024	0.298	0.156	52.4	0.223
16	2.0	1.2	1.074	1.45	2.78	0.024	0.596	0.156	26.2	0.149

TABLE 3. Conditions for experiments (ii): sodium hydroxide and nitric acid (see section 3.2). In all experiments, the Reynolds number at the source is $Re_0 = 1061$, the Schmidt number associated with the plume fluid is $Sc_b = 517$ (Noultly & Leaist 1984), and that associated with the ambient fluid is $Sc_a = 337$ (Yeh & Wills 1971).

<i>Exp.</i>	Q_0 ($\times 10^{-6}$)	r_0 ($\times 10^{-3}$)	ρ_b^0/ρ_a	B ($\times 10^{-7}$)	Γ_0 ($\times 10^{-2}$)	L_{M_0}	C_a	C_b^0 ($\times 10^{-3}$)	D_s	L_s
17	1.0	0.6	1.074	7.25	0.35	0.034	0.05	0.10	2.00×10^{-3}	0.016
18	1.0	0.6	1.074	7.25	0.35	0.034	0.10	0.10	9.99×10^{-4}	0.016
19	1.0	0.6	1.074	7.25	0.35	0.034	0.15	0.10	6.66×10^{-4}	0.016
20	1.0	0.6	1.074	7.25	0.35	0.034	0.20	0.10	5.00×10^{-4}	0.016
21	1.0	0.6	1.074	7.25	0.35	0.034	0.25	0.10	4.00×10^{-4}	0.016

TABLE 4. Conditions for experiments (iii): methylene blue and ascorbic acid (see section 3.3). In all experiments, the Reynolds number at the source is $Re_0 = 1061$, the Schmidt number associated with the plume fluid is $Sc_b = 1209$ (Leaist 1988), and that associated with the ambient fluid is $Sc_a = 880$ (Shamim & Baki 1980).

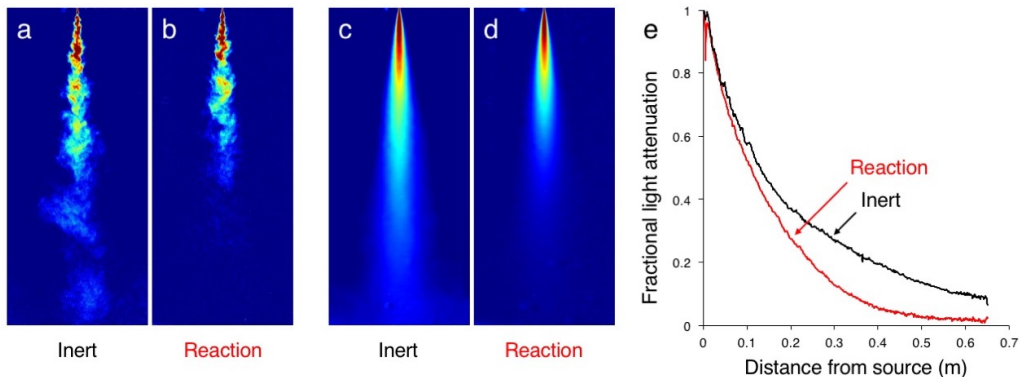


FIGURE 5. (a, b) Instantaneous and (c, d) time-averaged distributions of light attenuation produced by a plume of ammonium hydroxide descending through (a, c) fresh water or (b, d) a solution of acetic acid. A comparison of the time- and depth-averaged profiles of light attenuation along the plume’s centreline is given in panel (e).

221 the tank (see tables 1 and 4). Within the range of concentrations used, the chemical
 222 reaction between ascorbic acid and methylene blue did not affect the density of the
 223 solutions (Domingos & Cardoso 2015), nor the entrainment coefficient α (see section
 224 2.2 and appendix A). Inert sucrose was added to the plume fluid to increase its density
 225 relative to the ambient fluid. The products of the reaction between methylene blue and
 226 ascorbic acid are leucomethylene blue and dehydroascorbic acid,



227 Mowry & Ogren (1999) measured the rate law of this second-order reaction

$$r = k_{r_2} [\text{MB}] [\text{H}_2\text{A}] \quad (3.10)$$

228 and found $k_{r_2} \approx 1 \pm 0.2 \text{ M}^{-1} \text{ s}^{-1}$ at 20°C . Snehalatha *et al.* (1997) proposed two different
 229 mechanisms for the reaction between ascorbic acid and methylene blue. Both mechanisms
 230 are irreversible and second order. As a result of the irreversible reaction, the colour of
 231 a mixture of methylene blue and ascorbic acid gradually fades. In our experiments, we
 232 track the progress of the reaction in the plume by observing the change in the colour of
 233 the plume fluid (see section 5.4).

234 It should be noted that for the reaction to produce significant effects within a relatively
 235 short time during each experiment, sufficiently large concentrations of ascorbic acid and
 236 methylene blue were used in this set of experiments (see table 4). At these concentrations,
 237 the colour of the plume fluid near the source was very dark, making it difficult to measure
 238 the concentration of dye in the plume eddies using the light attenuation technique in this
 239 region. However, the colour of the plume fluid rapidly became lighter as the fluid became
 240 increasingly dilute while descending through the tank. For this reason, in plotting figures
 241 7d, 9 and 12 (sections 4 and 5), we will only consider the portion of the tank in which
 242 the concentration of dye in the plume fluid could be measured using the experimental
 243 technique described in section 2.

244 4. Experimental observations

245 4.1. Time-averaged concentration of the plume fluid

246 Figure 5 shows a side-by-side comparison of the outcomes of two experiments in which
 247 the same alkaline plume fluid descended through either fresh water or an acidic solution

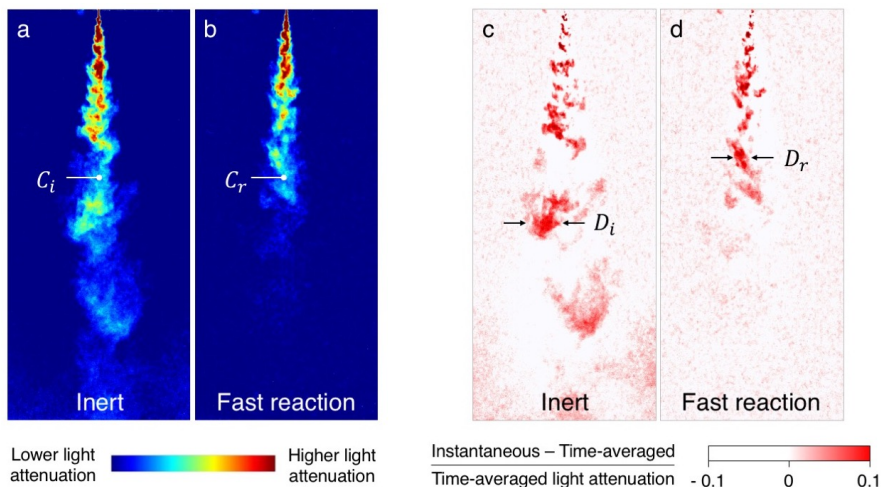


FIGURE 6. Instantaneous images of a fast-reaction, alkaline plume descending through (a) fresh water and (b) an acidic environment: a rainbow colormap is used to illustrate the distribution of the light attenuation in the tank. In figures (c) and (d), the same images are processed to highlight the descending eddies. A white/red colormap is used to highlight the regions of the plume in which the instantaneous dye concentration exceeds the time-averaged concentration.

248 (experiment 1 in table 2). In figures 5a and c, the tank was filled with fresh water. Both
 249 the instantaneous and the time-averaged images show that while descending through the
 250 tank, the plume fluid became increasingly dilute as a result of the entrainment of ambient
 251 fluid. Figures 5b and d illustrate the results of an experiment in which the tank was filled
 252 with a solution of acetic acid. In this case, the plume was subjected to both dilution
 253 and chemical reaction, leading to a faster reduction in the pH of the fluid, which in turn
 254 resulted in a faster reduction in the concentration of dye in the fluid (figure 5e).

255 The red line in figure 5e shows that at distances below the source larger than ap-
 256 proximately 0.45-0.50 m, the plume in the reactive system produced a negligible amount
 257 of light attenuation through the tank. At this distance from the source, all the phen-
 258olphthalein dye contained in the supplied fluid had turned colourless, and this indicates
 259 that the pH of the fluid had decreased beyond neutralisation as a result of the chemical
 260 reaction (see section 2.1, cf. Wittke 1983).

261 4.2. Distribution and concentration of the reactive fluid in plume eddies

262 While comparing the time-averaged concentration profiles depicted in figure 5e enables
 263 us to identify the distance from the source at which the chemical reaction is complete, we
 264 should note that turbulent plumes are effectively composed of transient or intermittent
 265 eddies (Mingotti & Woods 2015). It is interesting to observe how the concentration of
 266 the reactants varies in the eddies as a function of distance from the source and of the
 267 reaction rate.

268 In figure 6a, we use false colours to illustrate the distribution of the light attenuation
 269 produced by a dyed inert plume which descends through fresh water. In order to identify
 270 the turbulent eddies in this picture, we first subtract the time-averaged mean distribution
 271 of light attenuation from the instantaneous distribution depicted in the image. We then
 272 use a red colormap to illustrate the fractional amplitude of the fluctuations above
 273 the mean (figure 6c). We observe that as the inert plume fluid descends through fresh
 274 water, the diameter of the eddies, D_i , increases with distance from the source due to

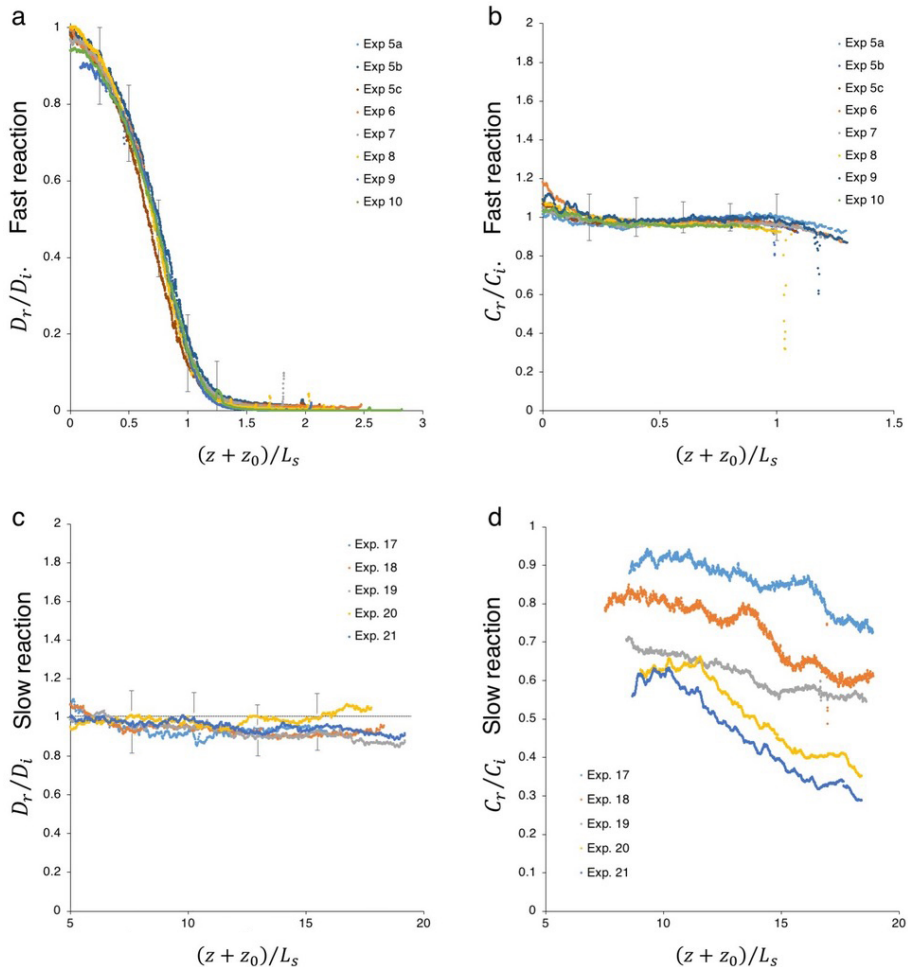


FIGURE 7. Time-averaged mean (a, c) size of the parcels of reactive fluid relative to the size of the eddies in an inert plume, D_r/D_i , and (b, d) concentration of dye per unit volume in a parcel of reactive fluid relative to the concentration in a parcel of inert plume fluid, C_r/C_i , for (a, b) fast and (c, d) slow reactions. All data are presented as a function of the distance from the virtual origin of the plume, scaled by the stoichiometric length scale, L_s , given by equation 5.13. Panels (a, b) show that the variation between the results of different experiments is larger at small distances below the source, $(z + z_0)/L_s < 0.3 - 0.4$ (i.e. $z < 4 - 6$ cm below the nozzle approximately, see tables 2 and 3). In this near-source region, the flow in the plume is still transitional or just settling into full turbulence. It should be noted that the magnitude of the discrepancies between the results depicted in panels (a, b) is typically smaller than the expected errors associated with the image analysis technique, as discussed in section 2.

275 the entrainment of ambient fluid (figure 6c, cf. Papanicolaou & List 1988), while the
 276 concentration of dye in the eddies, C_i , decreases as a result of dilution (figure 6a).

277 We repeat the same analysis for all the images captured during each experiment: as an
 278 example, figures 6b and d show the results obtained when processing one of the pictures
 279 captured during experiment 1 (fast reaction, see table 2). Using these figures, we measure
 280 the different sizes, D_r , and concentrations, C_r , of the parcels of dyed fluid in the reactive
 281 plume. Figure 7 illustrates the results of our measurements. It is seen that the mean
 282 diameter of the parcels of dyed fluid in a plume with a fast chemical reaction is similar to

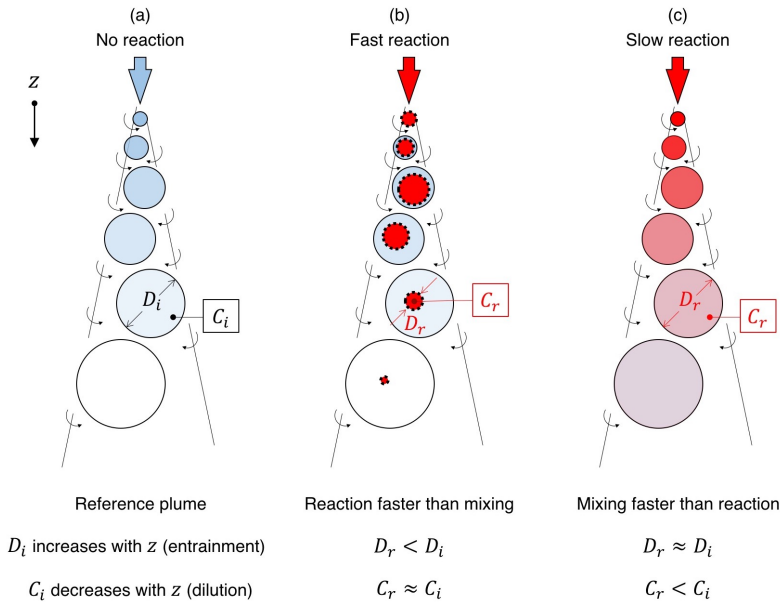


FIGURE 8. Cartoon illustrating the different distributions of reactants in the two cases of a fast and slow chemical reaction.

283 that of the eddies of an inert plume near the source; however, the ratio D_r/D_i decreases
 284 progressively with distance from the source (figure 7a). On the other hand, we observe
 285 that the mean light attenuation produced by a unit volume of dyed fluid in a plume with
 286 a fast chemical reaction is approximately equal to that produced by a unit volume of
 287 dyed fluid in an inert plume at all distances from the source, $C_r/C_i \approx 1$ (figure 7b).

288 The results obtained when analysing the pictures captured during the slow reaction
 289 experiments are different. Figure 7c shows that the size of the parcels of dyed fluid in
 290 a plume with a slow reaction was similar to that of the eddies in an inert plume at
 291 all distances from the source in our experiments, $D_r/D_i \approx 1$. On the other hand, the
 292 concentration of dye in a plume with a slow reaction decreased progressively with distance
 293 from the source relative to the concentration of dye in an inert plume, $C_r/C_i < 1$ (figure
 294 7d).

295 These experimental observations suggest that the process of consumption of the
 296 chemical species in a plume with a fast reaction is different than that in a plume with
 297 a slower reaction (see figure 8). When the time required for the reaction to develop is
 298 smaller than the time required for a parcel of dyed plume fluid to mix with the entrained
 299 fluid, then the reaction primarily takes place near the edges of the parcel (dashed black
 300 lines in figure 8b). In this border region, the dyed fluid mixes locally with the entrained
 301 fluid: as the two fluids react, the colour of the dyed fluid rapidly fades. This leads to
 302 a reduction in the diameter of the parcel of dyed reactive fluid, D_r , as illustrated in
 303 figure 7a. The fluid in the core of the parcel, however, is not affected by the fast chemical
 304 reaction, and so its concentration C_r is only subjected to the effects of dilution: hence,
 305 C_r decreases with distance from the source at a rate similar to that of the concentration
 306 of dye in an inert plume, C_i (see figure 7b).

307 On the other hand, in the case of a slower reaction, the time required for the convective
 308 mixing of the entrained fluid into an eddy is shorter than the time required for the
 309 reaction to develop. In this situation, the entrained reactants are continuously distributed

throughout the entire volume of the eddy, $D_r \sim D_i$ (figures 7c and 8c). The fluid in the bulk of the eddy is consequently subjected to the effects of both dilution and reaction, and so C_r decreases more rapidly than C_i with distance from the source (see figure 7d).

Motivated by these experimental results, in the next section we develop a simple model based on plume theory to quantify the concentration of the supplied reactants in the plume fluid as a function of distance from the source. We then test the model by comparing the outcome of the experiments with the model predictions.

5. Model

In this section, plume theory is used to build a model which quantifies the concentration of reactants in the plume fluid as a function of distance from the source in the two limiting cases of a slow and of an instantaneous reaction. In sections 5.1-5.3, we first estimate and compare the length and time scales which govern the processes of entrainment, dilution and chemical reaction within the plume. In section 5.4, we focus on relatively slow reactions, which develop on a time scale larger than that required for the convective mixing of the fluid in the plume. In section 5.5, we focus on fast reactions. We estimate the fraction of the entrained volume flux which mixes and reacts within the plume as a function of distance from the source. In the limit of an instantaneous reaction, we calculate the distance at which the reaction is complete.

5.1. Entrainment of ambient fluid

Plume theory indicates that as a result of entrainment of ambient fluid, the plume volume flux, Q ($\text{m}^3 \text{s}^{-1}$), increases with distance from the source z (Morton *et al.* 1956) as

$$Q = \lambda B^{\frac{1}{3}} z^{\frac{5}{3}} \quad (5.1)$$

where B ($\text{m}^4 \text{s}^{-3}$) is the buoyancy flux and

$$\lambda = \frac{6}{5} \alpha \left(\frac{9}{10} \alpha \right)^{\frac{1}{3}} \pi^{\frac{2}{3}} \quad (5.2)$$

is a universal constant dependent on the entrainment coefficient α (Linden 1990). Both the plume radius b and the mean diameter of the eddies in the plume increase linearly with distance from the source (Papanicolau & List 1988). Consequently, the mean speed of the fluid, u (m s^{-1}), decreases with distance from the source

$$u = \frac{Q}{\pi b^2} \sim \alpha^{-2} \lambda B^{\frac{1}{3}} z^{-\frac{1}{3}} \quad (5.3)$$

It follows that the turbulent motion of the plume fluid and the entrainment of ambient fluid into the plume are governed by the following length and time scales (cf. table 5)

$$L_e = \alpha z \quad (5.4)$$

and

$$\tau_e = \frac{L_e}{u} = \alpha^3 \lambda^{-1} B^{-\frac{1}{3}} z^{\frac{4}{3}} \quad (5.5)$$

5.2. Stoichiometric dilution of the supplied fluid

We let Q_0 ($\text{m}^3 \text{s}^{-1}$) denote the plume volume flux at the source. We assume that the supplied fluid contains an alkaline solution, MOH, and we let C_b^0 (M) denote the initial concentration of this solution. As the plume descends through the surrounding ambient,

	<i>Length scale L</i>	<i>Time scale τ</i>
Entrainment	αz	$\alpha^3 \lambda^{-1} B^{-\frac{1}{3}} z^{\frac{4}{3}}$
Mixing	$Sc_b^{-\frac{1}{2}} \alpha^{\frac{7}{4}} \lambda^{-\frac{3}{4}} \nu^{\frac{3}{4}} B^{-\frac{1}{4}} z^{\frac{1}{2}}$	$\ln Sc_b \cdot \alpha^{\frac{7}{2}} \lambda^{-\frac{3}{2}} \nu^{\frac{1}{2}} B^{-\frac{1}{2}} z$
Stoichiometry	$\lambda^{-\frac{3}{5}} Q_0^{\frac{3}{5}} B^{-\frac{1}{5}} (1 + D_s)^{\frac{3}{5}}$	$\alpha^2 \lambda^{-\frac{8}{5}} Q_0^{\frac{3}{5}} B^{-\frac{8}{15}} z^{\frac{1}{3}} (1 + D_s)^{\frac{3}{5}}$
Reaction	$\alpha^{-2} \lambda B^{\frac{1}{3}} z^{-\frac{1}{3}} (k_r C_a)^{-1}$	$(k_r C_a)^{-1}$

TABLE 5. Length and time scales used in the model.

344 the supplied fluid is diluted through the addition of a volume flux Q_e of entrained acid,
 345 HA, of a uniform concentration C_a . As indicated by Ulpre *et al.* (2013), the chemical
 346 reaction between the fluids is governed by the conservation of charge

$$[\text{H}^+] + [\text{M}^+] = [\text{OH}^-] + [\text{A}^-] \quad (5.6)$$

347 and by the conservation of mass of acid and alkali respectively

$$C_a Q_e = ([\text{AH}] + [\text{A}^-]) (Q_e + Q_0) \quad (5.7)$$

348

$$C_b^0 Q_0 = ([\text{MOH}] + [\text{M}^+]) (Q_e + Q_0) \quad (5.8)$$

349 We let K_a and K_b (M) denote the dissociation constants of the acidic and of the alkaline
 350 solutions respectively

$$K_a = \frac{[\text{A}^-] [\text{H}^+]}{[\text{AH}]} \quad (5.9)$$

351

$$K_b = \frac{[\text{M}^+] [\text{OH}^-]}{[\text{MOH}]} \quad (5.10)$$

352 We define the dilution coefficient D as the ratio between the volume flux of the en-
 353 trained fluid and that of the supplied fluid at a given distance from the source. Using a
 354 combination of equations 5.7-5.10, this coefficient is given by

$$D = \frac{C_b^0 K_b [\text{A}^-] (K_a + [\text{H}^+])}{C_a K_a [\text{M}^+] (K_b + [\text{OH}^-])} \quad (5.11)$$

355 As the volume flux of entrained fluid increases with distance from the source, the number
 356 of moles of entrained acid and the dilution coefficient also increase. We let D_s denote the
 357 critical stoichiometric dilution at which the supplied alkali and entrained acid are present
 358 in the plume in stoichiometric amounts. At this critical dilution, the mean concentration
 359 of hydrogen ions equals that of hydroxide ions in the solution, $[\text{H}^+] = [\text{OH}^-]$, and so
 360 using equations 3.6 and 5.6 we obtain

$$D_s = \frac{C_b^0 K_b (K_a + K_w^{1/2})}{C_a K_a (K_b + K_w^{1/2})} \quad (5.12)$$

361 Using a combination of equations 5.1 and 5.12, we calculate that the distance between
 362 the plume source and the level at which the stoichiometric dilution is achieved is given

363 by

$$L_s = \lambda^{-\frac{3}{5}} Q_0^{\frac{3}{5}} B^{-\frac{1}{5}} (1 + D_s)^{\frac{3}{5}} \quad (5.13)$$

364 as listed in table 5. Equations 5.3 and 5.13 are then used to estimate that the time
365 required for the plume fluid to flow from the source to the stoichiometric level scales by

$$\tau_s = \frac{L_s}{u} = \alpha^2 \lambda^{-\frac{8}{5}} Q_0^{\frac{3}{5}} B^{-\frac{8}{15}} z^{\frac{1}{3}} (1 + D_s)^{\frac{3}{5}} \quad (5.14)$$

366

5.3. Time scale for chemical reaction

367 In our experiments, the volumetric flow rate of ambient fluid entrained into the
368 plume becomes larger than that of source fluid at short distances from the source. The
369 concentration of the ambient chemical species in the plume is therefore approximately
370 constant in the plume, and the chemical reaction between the source and the entrained
371 fluid may be treated as a pseudo-first order reaction (Domingos & Cardoso 2015). The
372 time scale for a change in the concentration of the chemical species in the plume fluid is
373 therefore given by (see table 5)

$$\tau_r = (k_r C_a)^{-1} \quad (5.15)$$

374 while the distance travelled by the plume fluid during this time scales as

$$L_r = u\tau_r = \alpha^{-2} \lambda B^{\frac{1}{3}} z^{-\frac{1}{3}} (k_r C_a)^{-1} \quad (5.16)$$

375 We compare the time scale for achieving the stoichiometric dilution, τ_s , with the
376 reaction time scale, τ_r , in our experiments. In the slow reaction experiments (see section
377 3.3 and table 4), the ratio τ_s/τ_r is typically of order $10^{-3} - 10^{-2}$. This indicates that
378 the plume rapidly entrains a large amount of ambient fluid while descending to the
379 stoichiometric level L_s ; however, the chemical reaction is comparatively slow. Hence, we
380 expect the consumption of the supplied chemicals to be controlled by the reaction time
381 scale (see table 5), and most of the effects of the reaction to be visible at distances
382 larger than L_s . On the other hand, in our fast reaction experiments (see sections 3.1-
383 3.2 and tables 2-3), τ_s/τ_r is typically of order $10^7 - 10^8$. This suggests that as soon as
384 a parcel of acidic fluid is entrained from the ambient and mixed within the plume, it
385 immediately reacts with the descending fluid. Hence, we expect the consumption of the
386 supplied chemicals to be controlled by the entrainment and mixing time scales (see table
387 5), and most of the effects of the reaction to be visible at distances smaller than L_s .

388

5.4. Consumption of the chemical species in a plume with a slow reaction

389 In this section, we focus on slow reactions and quantify the concentration of the
390 supplied chemicals in the plume fluid as a function of distance from the source. Both
391 dilution and reaction lead to a gradual reduction in the concentration of the supplied
392 chemical species C_b (cf. Domingos & Cardoso 2013). Using equations 5.1 and 5.15, this
393 concentration varies with time according to

$$\frac{dC_b}{dt} = -\frac{5}{4} \frac{C_b}{t} - \frac{C_b}{\tau_r} \quad (5.17)$$

394 The ratio between the concentration in a reactive system ($C_a > 0, \tau_r > 0$) and that in
395 an inert system ($C_a = 0, \tau_r \rightarrow \infty$) is then

$$\frac{C_{b,\text{reaction}}}{C_{b,\text{inert}}} = \exp\left(-\frac{t}{\tau_r}\right) \quad (5.18)$$

396

Our model of the consumption of reactants in a plume with a slow chemical reaction is

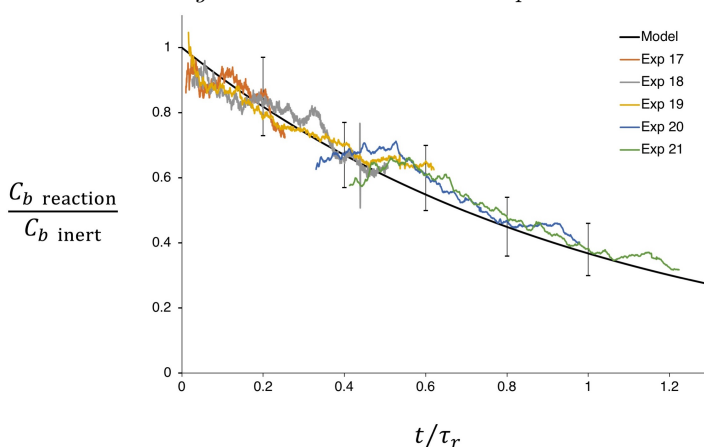


FIGURE 9. Comparison between the results of the slow reaction experiments (coloured lines) and the prediction of the model (black line, based on equation 5.18).

397 tested against the results of the laboratory experiments described in section 3.3. For each
 398 of the experiments listed in table 4, we calculate the ratio between the time-averaged
 399 light attenuation produced by a methylene blue plume which descends through an acidic
 400 environment, and that produced by the associated inert plume which descends through
 401 fresh water (cf. figure 7d). Figure 9 shows that the model prediction (black line, based on
 402 equation 5.18) is in good agreement with the results of the experiments, with deviations
 403 of order 10%, which are compatible with the expected errors associated with the image
 404 processing technique (see section 2.2).

405 5.5. Consumption of the chemical species in a plume with a fast reaction

406 We now consider the case of a fast reaction between the supplied and the entrained
 407 fluid in the plume. In the limit $\tau_s/\tau_r \gg 1$, we assume the reaction to be instantaneous
 408 ($\tau_r = L_r = 0$), and the supplied chemical species to be progressively consumed in the
 409 region $0 < z < L_s$ as an increasing flux of ambient fluid is entrained and mixed within
 410 the plume.

411 Domingos & Cardoso (2015) previously observed non-uniform distributions of reactants
 412 in single-phase thermals with a fast reaction, and found the progress of the reaction to be
 413 controlled by the local mixing of the reactive fluids. Similarly, in section 4.2 we observed
 414 that sufficiently fast reactions may only develop in a portion of the plume's volume, with
 415 chemically active regions near the edges of each parcel of reactive fluid, and inactive
 416 regions in the core of each parcel of fluid (see figure 8b). Based on these experimental
 417 observations and on the previous findings by Domingos & Cardoso, we let τ_m denote the
 418 time scale for the local mixing of the fluids at the Batchelor scale (Batchelor 1959; Fox
 419 2003),

$$420 \tau_m = \frac{1}{2} \ln Sc_b \tau_e Re^{-\frac{1}{2}} \sim \ln Sc_b \cdot \alpha^{\frac{7}{2}} \lambda^{-\frac{3}{2}} \nu^{\frac{1}{2}} B^{-\frac{1}{2}} z \quad (5.19)$$

421 in which Sc_b is the Schmidt number associated with the plume (see tables 2 and 3), ν
 422 ($\text{m}^2 \text{s}^{-1}$) is the kinematic viscosity of the mixture (Pope 2000; Kundu *et al.* 2015), and

$$423 Re = \frac{uL_e}{\nu} = \alpha^{-1} \lambda \nu^{-1} B^{\frac{1}{3}} z^{\frac{2}{3}} \quad (5.20)$$

424 is the Reynolds number associated with the plume eddies. For each of our experiments,
 425 we calculate τ_m as a function of distance from the source using equation 5.19 and the

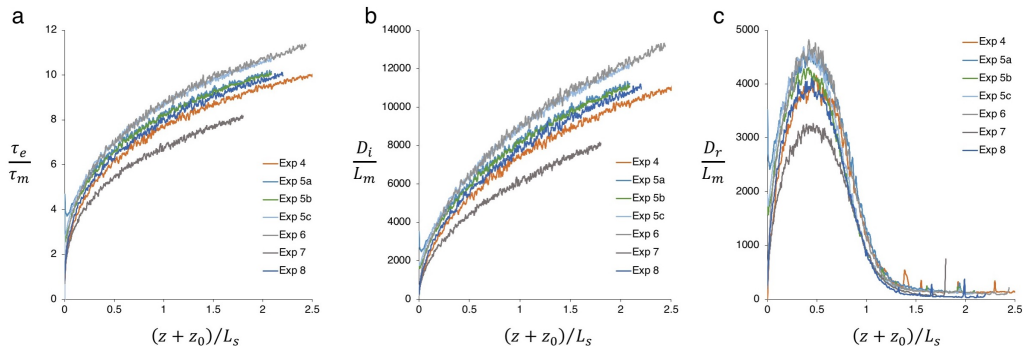


FIGURE 10. Experimental measurements of (a) the ratio between the time scale for convective mixing of the fluid in an eddy and the Batchelor time scale, τ_e/τ_m (Batchelor 1959; Fox 2003); (b) the ratio between the time-averaged mean diameter of the eddies and the Batchelor length scale, D_i/L_m ; and (c) the ratio between the time-averaged mean diameter of the parcels of reactive fluid and the Batchelor length scale, D_r/L_m . All data are presented as a function of the distance from the virtual origin of the plume, scaled by L_s (equation 5.13).

424 experimental measurements of the speed and size of the eddies in the plume (see section
 425 2.2). Figure 10a shows that the time required for the turbulent convection of the fluid
 426 in an eddy is always much larger than the time required for the local mixing of the fluid
 427 at the Batchelor scale in our experiments, $\tau_e \gg \tau_m$. Hence, we expect that fast chemical
 428 reactions will develop primarily at this latter scale, and that the depth of the chemically
 429 active region in the periphery of each parcel of reactive fluid will be controlled by the
 430 Batchelor length scale, L_m (Batchelor 1959; Fox 2003)

$$L_m = Sc_b^{-\frac{1}{2}} L_e Re^{-\frac{3}{4}} = Sc_b^{-\frac{1}{2}} \alpha^{\frac{7}{4}} \lambda^{-\frac{3}{4}} \nu^{\frac{3}{4}} B^{-\frac{1}{4}} z^{\frac{1}{2}} \quad (5.21)$$

431 For each experiment with a fast reaction, L_m is estimated using equation 5.21 and the
 432 experimental measurements of the time-averaged speed and size of the eddies in the
 433 plume (see section 2.2). In figures 10b and c, we compare L_m with the mean diameters
 434 of the eddies, D_i , and of the parcels of reactive fluid in our experiments, D_r (see figure
 435 6). It is seen that in the region $0 < z < L_s$, the Batchelor length scale is much smaller
 436 than both diameters: this is consistent with our experimental observation of the chemical
 437 reaction developing in a relatively thin region near the edge of each parcel of reactive
 438 fluid in the plume (see figure 8b). The mixture of ambient and entrained fluid in this
 439 region rapidly becomes neutralised, leading to a reduction in the parcel's size (see figure
 440 7). As a result of the slower process of large-scale mixing, some of the neutralised fluid
 441 is subsequently entrained and diluted into the core of the parcel of fluid; however, we
 442 expect that no chemical reaction will develop there.

443 Using equations 5.19 and 5.21, we estimate that the volume flux of entrained fluid
 444 which mixes with the plume fluid in a unit of time, herein denoted by Q_m , scales by

$$\frac{dQ_m}{dt} \sim \frac{L_m^3}{\tau_m^2} = \frac{\alpha^{-\frac{7}{4}} \lambda^{\frac{3}{4}} \nu^{\frac{5}{4}} B^{\frac{1}{4}} z^{-\frac{1}{2}}}{Sc_b^{\frac{3}{2}} (\ln Sc_b)^2} \quad (5.22)$$

445 In turn, plume theory indicates that the volume flux of ambient fluid which is entrained
 446 by the plume in a unit of time increases with distance from the source according to

$$\frac{dQ}{dt} \sim \frac{L_e^3}{\tau_e^2} = \alpha^{-3} \lambda^2 B^{\frac{2}{3}} z^{\frac{1}{3}} \quad (5.23)$$

447 At all times, the volume flux of entrained fluid which mixes within the plume must be

448 smaller or equal to the volume flux of fluid which is entrained from the ambient,

$$\frac{dQ_m}{dt} \leq \frac{dQ}{dt} \quad (5.24)$$

449 Using equations 5.22 and 5.23, we estimate that the fraction of the entrained volume
450 flux which mixes and reacts with some of the supplied fluid in the plume decreases with
451 distance from the source

$$\frac{dQ_m}{dQ} = \min \left(\frac{\alpha^{\frac{5}{4}} \beta \lambda^{-\frac{5}{4}} \nu^{\frac{5}{4}} B^{-\frac{5}{12}} z^{-\frac{5}{6}}}{Sc_b^{\frac{3}{2}} (\ln Sc_b)^2}; 1 \right) \quad (5.25)$$

452 in which β is a dimensionless constant. Equation 5.25 indicates that a critical distance
453 from the source exists, at which the volume flux of fluid which is entrained by the plume
454 is equal to that which is mixed by the small-scale turbulence

$$z_{\text{crit}} = \left(\frac{\beta^3}{Sc_b^2 (\ln Sc_b)^6} \right)^{\frac{2}{5}} \frac{L_m^2}{L_e} \quad (5.26)$$

455 For $z < z_{\text{crit}}$, the volume of fluid entrained by the plume is smaller than the maximum
456 volume which can be mixed at the Batchelor scale: we therefore expect that all the fluid
457 entrained by the plume will mix with a portion of the supplied plume fluid and react,
458 but the overall progress of the reaction will be limited by the lack of entrained fluid. On
459 the other hand, for $z > z_{\text{crit}}$ the volume of fluid which is entrained by the plume is larger
460 than the maximum volume which can be mixed at the Batchelor scale: in this case, the
461 reaction will only develop in a fraction of the entrained fluid due to incomplete mixing.

462 Equation 5.26 suggests that in case $z_{\text{crit}} < L_s$, only a fraction of the entrained fluid will
463 react with the supplied fluid in the region $z_{\text{crit}} < z < L_s$. Consequently, the consumption
464 of the chemical species will be reduced in this region, and the distance from the source
465 at which the chemical reaction reaches completion, z_r , will be larger than L_s (equation
466 5.13). To estimate this distance, we let R denote the fraction of the supplied chemicals
467 which are still reactive at a given distance from the source. Using equations 5.12, 5.25
468 and 5.26, we calculate that this fraction is given by

$$R(z) = \begin{cases} 1 - \frac{Q(z)}{(1 + D_s) Q_0}, & 0 < z < z_{\text{crit}} \\ 1 - \frac{1}{(1 + D_s) Q_0} \left(\lambda B^{\frac{1}{3}} z_{\text{crit}}^{\frac{5}{3}} + \int_{z_{\text{crit}}}^z \frac{\alpha^{\frac{5}{4}} \beta \nu^{\frac{5}{4}} B^{-\frac{5}{12}} z^{-\frac{5}{6}}}{\lambda^{\frac{5}{4}} Sc_b^{\frac{3}{2}} (\ln Sc_b)^2} \frac{dQ}{dz} dz \right), & z_{\text{crit}} < z < z_r. \end{cases} \quad (5.27)$$

469 A combination of equations 5.1, 5.13 and 5.27 enables us to write R as a function of the
470 stoichiometric length scale, L_s , and the critical distance, z_{crit}

$$R(z) = \begin{cases} 1 - \left(\frac{z}{L_s} \right)^{\frac{5}{3}}, & 0 < z < z_{\text{crit}} \\ 1 + \left(\frac{z_{\text{crit}}}{L_s} \right)^{\frac{5}{3}} - 2 \left(\frac{z}{L_s} \right)^{\frac{5}{6}} \left(\frac{z_{\text{crit}}}{L_s} \right)^{\frac{5}{6}}, & z_{\text{crit}} < z < z_r. \end{cases} \quad (5.28)$$

471 Equation 5.28 indicates that the fraction of reactive chemicals in the plume decreases
472 more rapidly in the region $0 < z < z_{\text{crit}}$, where all of the entrained fluid mixes with the
473 descending fluid and reacts; however, for $z_{\text{crit}} < z < z_r$, some of the entrained fluid does
474 not react due to incomplete mixing, and so R decreases more slowly in this region. Using
475 equation 5.27, we calculate that the distance from the source at which the instantaneous

476 reaction reaches completion ($R = 0$) is given by

$$z_r = \left[\frac{(1 + D_s) Q_0 + \alpha^{\frac{5}{2}} \beta^2 \lambda^{-\frac{3}{2}} S c_b^{-3} (\ln S c_b)^{-4} \nu^{\frac{5}{2}} B^{-\frac{1}{2}}}{2 \alpha^{\frac{5}{4}} \beta \lambda^{-\frac{1}{4}} S c_b^{-\frac{3}{2}} (\ln S c_b)^{-2} \nu^{\frac{5}{4}} B^{-\frac{1}{2}}} \right]^{\frac{6}{5}} \quad (5.29)$$

477 The ratio between this distance and the stoichiometric length scale is then obtained from
478 equation 5.28

$$\frac{z_r}{L_s} = 2^{-\frac{6}{5}} \left[\left(\frac{z_{\text{crit}}}{L_s} \right)^{\frac{5}{6}} + \left(\frac{z_{\text{crit}}}{L_s} \right)^{-\frac{5}{6}} \right]^{\frac{6}{5}} \quad (5.30)$$

479 As expected, equation 5.30 indicates that $z_r/L_s = 1$ when $z_{\text{crit}} = L_s$ so that all the fluid
480 entrained by the plume mixes with the supplied fluid while descending from the source
481 to the stoichiometric level. However, for $z_{\text{crit}} < L_s$ some of the entrained fluid does
482 not immediately react within the plume, and this results in an increase in the distance
483 required for the consumption of the supplied chemical species, $z_r/L_s > 1$.

484 Our model of the consumption of reactants in a plume with a fast chemical reaction
485 is tested against the results of the laboratory experiments described in sections 3.1 and
486 3.2. In doing so, we first use our measurements of the mean size of the inert and reactive
487 parcels of fluid in the plume (D_i and D_r respectively, see figure 7a) to estimate the
488 value of the dimensionless coefficient β introduced in equation 5.25. We then use this
489 value and equation 5.30 to calculate the expected level at which the chemical reaction
490 reaches completion, and we compare the prediction of the model with the outcome of the
491 experiments.

492 While estimating the value of β in our experiments, we assume as an approximation
493 that the volume of each parcel of fluid in the plume is proportional to the third power of
494 the diameter of the parcel. It follows that as the plume entrains fluid from the surrounding
495 ambient, the mean diameter of the plume eddies, D_i , increases with distance from the
496 source according to

$$\frac{dQ}{dz} \approx \frac{1}{\tau_e} \frac{dD_i^3}{dz} \quad (5.31)$$

497 A fraction of the entrained fluid mixes and reacts within the plume, leading to a reduction
498 in the mean diameter of the parcels of reactive fluid (see figure 8b). Using equations 5.12
499 and 5.22, we estimate that D_r decreases with distance from the source according to

$$\left(\frac{1 + D_s}{D_s} \right) \frac{dQ_m}{dz} \approx - \frac{4\pi D_r^2}{\tau_m} \frac{dD_r}{dz} \quad (5.32)$$

500 Using a combination of equations 5.25, 5.31 and 5.32, we obtain

$$\frac{\beta}{S c_b^{\frac{3}{2}} (\ln S c_b)^2} \left(\frac{\alpha^{\frac{5}{4}} \nu^{\frac{5}{4}}}{\lambda^{\frac{5}{4}} B^{\frac{5}{12}} z^{\frac{5}{6}}} \right) \approx - \frac{4}{3} \frac{\pi D_s}{(1 + D_s)} \left(\frac{D_r^2 \tau_e}{D_i^2 \tau_m} \right) \frac{dD_r}{dD_i} + c_1 \quad (5.33)$$

501 Equation 5.33 and the results of the experiments described in sections 3.1 and 3.2 are
502 used to plot figure 11a. It is seen that for $z_{\text{crit}} < z < z_r$, the data collected during a
503 number of different experiments collapse onto a line: by measuring the slope of this line,
504 we estimate that $\beta S c_b^{-\frac{3}{2}} (\ln S c_b)^{-2} \approx (2.0 \pm 0.14) \times 10^4$ in our experiments. It should be
505 noted that since equations 5.31-5.33 are based on the approximation that the volume of
506 each parcel of fluid in the plume is proportional to the third power of the diameter of the
507 parcel and involve a derivative of the experimental measurements, we should not expect
508 the collapse of the experimental results depicted in figure 11a to be perfect. Furthermore,

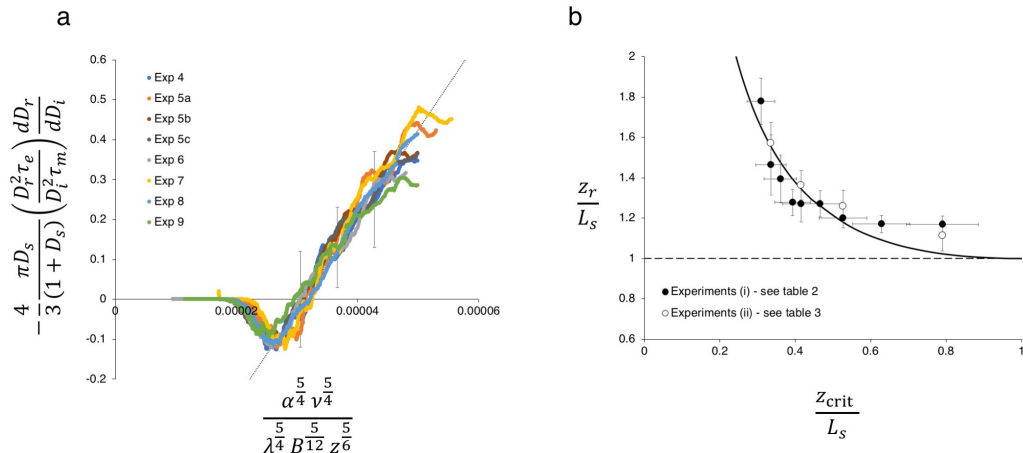


FIGURE 11. (a) We use equation 5.33 to estimate the value of β in our experiments, based on the measurements of D_i and D_r illustrated in figure 7; (b) Equation 5.30 and the measured constant $\beta S c_b^{-3/2} (\ln S c_b)^{-2}$ are then used to estimate the distance below the source at which the instantaneous acid-base reaction is complete, z_r (solid line). Close and open circles are used to illustrate the results of experiments (i) and (ii) respectively (see tables 3 and 2). In plotting the symbols, horizontal error bars are included to illustrate the impacts of a $\pm 10\%$ deviation in the value of β .

509 equation 5.33 only applies to the region of the flow in which the mixing of the entrained
 510 fluid is incomplete, and is not applicable to the near-source region, $0 < z < z_{\text{crit}}$ (see
 511 equation 5.25). For this reason, we do not expect the vertical intercepts of the sloping
 512 lines in figure 11a to be equal to zero, and a dimensionless constant c_1 has been added to
 513 equation 5.33 accordingly. Since both the buoyancy flux B ($\text{m}^4 \text{s}^{-3}$) and the viscosity ν
 514 ($\text{m}^2 \text{s}^{-1}$) were typically of order 10^{-6} in our experiments (see tables 2 and 3), we calculate
 515 that $z_{\text{crit}} \approx 0.10$ m in our experiments (equation 5.26). This implies that $z_{\text{crit}} < L_s$ in
 516 most of the experiments listed in tables 2 and 3.

517 The estimated value of β and equation 5.30 are used to calculate how the ratio z_r/L_s
 518 changes as a function of z_{crit}/L_s . In figure 11b, the prediction of the model (solid line)
 519 is compared with the results of the experiments (symbols). For each experiment, we
 520 detect the distance from the virtual source at which the time-averaged light attenuation
 521 produced by the reactive plume (red line in figure 5e) is 20 times smaller than that
 522 produced by the inert plume (black line in figure 5e). At this particular threshold, the light
 523 attenuation produced by the reactive plume is too faint to be perceived with the naked
 524 eye, but it can be captured and quantified using the image analysis technique described
 525 in section 2. At larger distances from the source, however, our experimental technique
 526 becomes less accurate as the signal-to-noise ratio of the light attenuation produced by
 527 the reactive plume decreases. For each experiment, the measured distance is scaled by
 528 the stoichiometric length scale L_s , and the result is plotted in figure 11b using an open
 529 or closed circle. It is seen that our experimental results compare well with the predictions
 530 of the model, with discrepancies of order 5 – 10% approximately.

531 5.6. Light attenuation profiles obtained in case of a fast or a slow reaction

532 The ratio between the critical distance z_{crit} and the stoichiometric length scale L_s can
 533 be given as a function of the entrainment, mixing and stoichiometric time scales (see

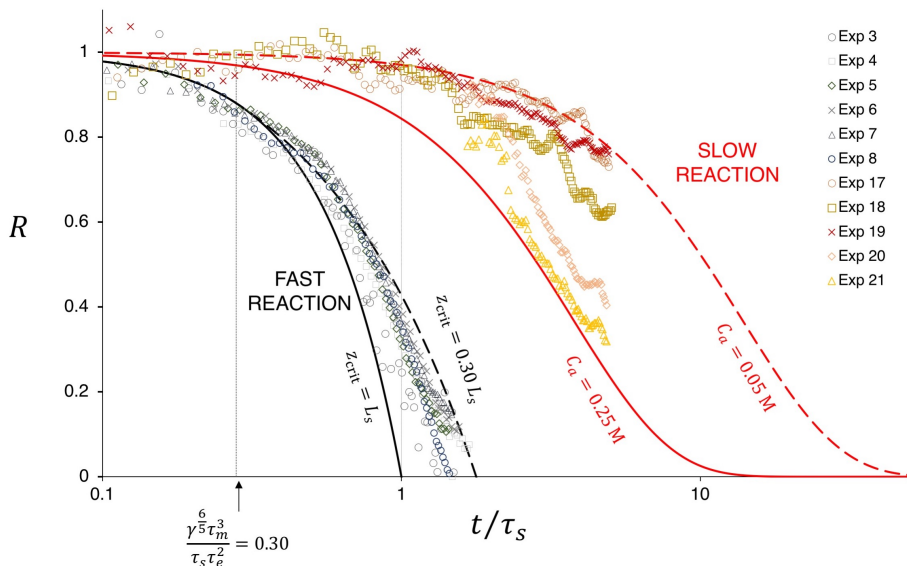


FIGURE 12. Fraction of the supplied chemicals which are still reactive in the plume, R , as a function of time. Equations 5.18 and 5.36 are used to plot the model predictions for slow- and fast-reaction experiments (red and black lines respectively). Symbols are used to illustrate the ratio between the time-averaged mean light attenuation produced by a reactive plume and that produced by an inert plume as measured during our experiments. On the horizontal axis, time is scaled by the stoichiometric time scale τ_s given by equation 5.14.

534 table 5)

$$\frac{z_{\text{crit}}}{L_s} = \frac{\gamma^{\frac{6}{5}} \tau_m^3}{\tau_s \tau_e^2} \quad (5.34)$$

535 in which

$$\gamma = \frac{\beta}{Sc_b^{\frac{3}{2}} (\ln Sc_b)^{\frac{9}{2}}} \quad (5.35)$$

536 is used for convenience. Using equations 5.28 and 5.34, the fraction of the supplied
 537 chemicals which is still reactive at a distance z below the source, R , is given as a function
 538 of the time t required for the plume fluid to flow from the source to z , as

$$R(t) = \begin{cases} 1 - \left(\frac{t}{\tau_s}\right)^{\frac{5}{3}}, & 0 < \frac{t}{\tau_s} < \frac{\gamma^{\frac{6}{5}} \tau_m^3}{\tau_s \tau_e^2} \\ 1 + \frac{\gamma^2 \tau_m^5}{\tau_s^{\frac{5}{3}} \tau_e^{\frac{10}{3}}} - \frac{2\gamma \tau_m^{\frac{5}{2}}}{\tau_s^{\frac{5}{6}} \tau_e^{\frac{5}{3}}} \left(\frac{t}{\tau_s}\right)^{\frac{5}{6}}, & \frac{\gamma^{\frac{6}{5}} \tau_m^3}{\tau_s \tau_e^2} < \frac{t}{\tau_s} < \frac{t_r}{\tau_s}. \end{cases} \quad (5.36a, b)$$

539 In equation 5.36, t_r denotes the time required for the plume fluid to flow from the source
 540 to the level at which the instantaneous chemical reaction reaches completion, z_r . Using
 541 a combination of equations 5.30 and 5.34, we calculate that this time lapse is given by

$$\frac{t_r}{\tau_s} = \left(\frac{\gamma^2 \tau_m^5 + \tau_s^{\frac{5}{3}} \tau_e^{\frac{10}{3}}}{2\gamma \tau_m^{\frac{5}{2}} \tau_s^{\frac{5}{6}} \tau_e^{\frac{5}{3}}} \right)^{\frac{6}{5}} \quad (5.37)$$

542 Equation 5.36a is used to plot the black solid curve in figure 12. This line illustrates the
 543 theoretical prediction of the minimum fraction of reactive chemicals in the plume fluid,

544 $R(t)$, in case the chemical reaction is instantaneous and mixing is complete ($z_{\text{crit}} \geq L_s$).
 545 This theoretical prediction is compared with the results of a number of fast reaction
 546 experiments (black and grey symbols, experiments 3-7 in table 2). Each symbol in the
 547 figure illustrates the ratio between the time- and depth-averaged mean intensity of light
 548 attenuation produced by a reactive plume and that produced by the associated inert
 549 plume at a given height in the tank during an experiment. It is seen that at small
 550 distances and times from the source ($t/\tau_s < 0.3 - 0.5$ and $R > 0.7 - 0.8$ approximately),
 551 there is a relatively good agreement between the results of the experiments and the
 552 model prediction illustrated by the black solid curve. However, for $t/\tau_s > 0.5$ and
 553 $R < 0.7$ approximately, the experimental results deviate from the black solid curve:
 554 in this region, the mean concentration of reactive chemicals in the plume fluid in our
 555 experiments is larger than that predicted by equation 5.36a as a result of incomplete
 556 mixing. Given that $z_{\text{crit}}/L_s > 0.30$ in all of our fast-reaction experiments (see figure
 557 11b), we use equation 5.36b to plot the dashed black curve in figure 12, which illustrates
 558 the theoretical prediction for $R(t)$ in case $z_{\text{crit}}/L_s = 0.30$. Figure 12 shows that most of
 559 the data points collected during the fast reaction experiments lie between the two black
 560 curves, as expected.

561 In figure 12, the model predictions and the results of our slow reaction experiments
 562 are plotted for comparison. For $\tau_s/\tau_r \ll 1$, we assume that the chemical species are
 563 well-mixed within the plume fluid (see section 2); this in turn implies that R equals the
 564 ratio between the concentration of dye in the reactive plume fluid and that in the inert
 565 plume fluid, $C_{b,\text{reaction}}/C_{b,\text{inert}}$. We therefore use equation 5.18 to plot the solid and the
 566 dashed red curves in figure 12: these lines illustrate the two bounding profiles associated
 567 with the maximum and minimum concentrations of reactants in the ambient fluid in our
 568 experiments. It is seen that all experimental results (yellow and red symbols, experiments
 569 17-21 in table 4) lie between these two bounding profiles as expected. Figure 12 shows
 570 that in the slow reaction experiments, a considerable amount of time is required for the
 571 consumption of the chemical species in the plume, and most of the reaction develops
 572 at times larger than τ_s , i.e. at distances larger than L_s below the source. Furthermore,
 573 as the concentration of the supplied chemical species in the plume fluid decreases, the
 574 rate of the pseudo-first order reaction also decreases. As indicated by equation 5.18, the
 575 pseudo-first order reaction only reaches completion when $t \rightarrow \infty$.

576 6. Conclusions

577 We have explored the behaviour of a reactive turbulent plume in the two limiting
 578 cases of (i) a slow reaction, which develops on a time scale longer than the time required
 579 for the entrained fluid to be mixed in the plume; and (ii) a faster reaction, which
 580 develops in a fraction of the mixing time. New experiments have been carried out using
 581 light-attenuation techniques for selected acid-base and redox chemical reactions. The
 582 measurements show that when the reaction is sufficiently slow, the entrained and source
 583 chemicals are rapidly mixed, and the reaction takes place throughout the entire volume
 584 of each eddy in the plume. However, faster reactions develop only at the periphery of each
 585 eddy, where the plume and the entrained fluids are mixed locally at the Batchelor scale
 586 (see figure 8b). The mixture of fluids in this border region becomes rapidly neutralised,
 587 while the concentration of reactants in the core of the parcel is not affected by the
 588 reaction.

589 Motivated by the experimental results, we have developed a model which quantifies the
 590 fraction of the entrained fluid that reacts with the source fluid in the plume. Our model
 591 indicates that the volume flux of entrained fluid increases with distance from the source

(see equation 5.23), while the volume flux of fluid which is mixed within the plume at the Batchelor scale decreases with distance from the source (see equation 5.22). Hence, a critical level z_{crit} exists at which the two fluxes are equal (see equation 5.26). In the region spanning between the plume source and this critical level, $z < z_{\text{crit}}$, the entire flux of entrained fluid is mixed locally and reacts within the plume, and so the progress of the reaction is limited by entrainment. However, at larger distances from the source, $z > z_{\text{crit}}$, only a fraction of the entrained fluid is mixed locally within the plume, and the progress of the reaction is limited by incomplete mixing. The experimental measurements of the average size of the plume eddies, D_i , and of the average size of the parcels of reactive fluid in the plume, D_r (see figure 7), have enabled us to quantify z_{crit} as a function of dimensionless coefficient β (see equation 5.26 and figure 11a). As a result of the non-uniform mixing of the fluids in the plume, the distance from the source at which an instantaneous reaction is complete, z_r , is larger than that predicted using the classical plume theory, L_s . Both the longitudinal concentration profile of source chemical in the plume and the ratio z_r/L_s are shown to depend on $(z_{\text{crit}}/L_s)^{5/6}$.

Appendix A. Turbulent properties of the flow

A.1. Source Reynolds number, entrainment coefficient

In each of our experiments, a turbulent, negatively-buoyant plume was formed by supplying relatively dense, dyed fluid through the nozzle located at the top of the tank (see figure 1). Based on the known source volume flux Q_0 and nozzle radius r_0 (see tables 2-4), we estimate that the mean flow speed at the nozzle was $u_0 = 0.45 \text{ m s}^{-1}$ in experiments 1-16 (tables 2 and 3) and $u_0 = 0.88 \text{ m s}^{-1}$ in experiments 17-21 (table 4). We then estimate the associated Reynolds number to be $Re_0 = 1061$ (see tables 2-4). It is seen that our experiments were conducted under Re conditions comparable or exceeding those of many published studies on turbulent plumes, including: George *et al.* (1977), $Re_0 = 870$; Papanicolau & List (1988), $Re_0 = 600$; Woods & Caulfield (1992), $Re_0 \approx 200$, here the authors note that the flow was laminar at the source, but became fully turbulent 2-3 cm below the source; and Ulpre *et al.* (2013), $Re_0 = 399$.

The time-averaged, mean velocity of the fluid descending along the plume centreline at larger distances from the source was measured in a number of experiments using the procedure described in section 2.2. Figure 3c shows that the measured velocities decrease with distance from the source in agreement with the theoretical prediction for fully turbulent plumes (Morton *et al.* 1956).

As described in section 2.2, two filling-box experiments were performed in the tank to quantify the entrainment coefficient α (cf. Linden *et al.* 1990). During these experiments, the tank was initially filled with fresh water and relatively dense, dyed inert fluid was supplied through the nozzle. The supplied fluid descended through the tank in the form of a plume, and eventually accumulated at its base. As a result, the tank became stratified, with a sharp interface separating the clear fluid at the top of the tank from the dyed fluid underneath. During each filling box experiment, we measured the rising speed of this interface, and used the collected data to estimate the volume flux in the plume as a function of distance from the source, $Q(z)$. In both experiments, we found that $Q(z) \sim z^{5/3}$, as predicted by the classical theory of turbulent plumes (Morton *et al.* 1956). We then used the measured flow rates to estimate $\alpha = 0.10 \pm 0.02$ (see section 2.2), which is consistent with the literature for turbulent plumes.

639 The results of the filling box experiments also enabled us to quantify the time scale for
 640 the experimental tank to become contaminated during an experiment. Given that the
 641 buoyancy flux B in our experiments was typically of order $10^{-6} \text{ m}^4 \text{ s}^{-3}$ (see tables 2-4),
 642 and given that the height of the tank was $H = 0.7 \text{ m}$ (see figure 1), the maximum volume
 643 flux in the plume at base of the tank was of order $Q_{max} \approx 5 \cdot 10^{-5} \text{ m}^3 \text{ s}^{-1}$ (see equation
 644 5.1). Since the volume of ambient fluid in the tank was of order 0.12 m^3 , we estimate the
 645 filling time scale to be larger than 2400 s (40 min) approximately. As discussed in section
 646 2.1, each of our experiments typically lasted 2.5-3 minutes. We therefore conclude that
 647 the impact of environmental stratification was negligible during our experiments.

648 A.2. Impacts of source momentum flux

650 As discussed in section 2.1, the source plume fluid was supplied to the experimental
 651 tank using a peristaltic pump; hence, the source volume and momentum fluxes were
 652 finite. In order to estimate the impacts of the source conditions, for each experiment
 653 listed in tables 2-4, we calculate the Morton number Γ_0 (Hunt & van den Bremer 2011)

$$\Gamma_0 = \frac{5BQ_0^2}{8\alpha\pi^{\frac{1}{2}}M_0^{\frac{3}{2}}} \quad (\text{A } 1)$$

654 Tables 2-4 show that in our experiments Γ_0 was of order 10^{-2} ; this indicates that our
 655 plumes were forced at the source, and that at small distances from the source the
 656 momentum $M(z)$ was larger than that of a pure plume. As a result, the descending
 657 flow behave like a buoyant jet in the near-source region. Following Hunt & van den
 658 Bremer (2011), we calculate the length scale L_{M_0} for the region in which the flow was
 659 affected by the initial momentum

$$L_{M_0} = M_0^{\frac{3}{4}} B^{-\frac{1}{2}} \quad (\text{A } 2)$$

660 Tables 2-4 show that the source momentum flux M_0 only affected the flow in the first
 661 2-3 cm below the nozzle, while beyond this region the flow in the 70cm-tall tank was
 662 governed by buoyancy. As described in section 2.2, the virtual origin of the flow, z_0 , was
 663 calculated in order to account for the impacts of the source conditions. Tables 2-4 also
 664 show that the stoichiometric length L_s was much larger than L_{M_0} in our experiments,
 665 indicating that our measurements of the critical distance from the source at which the
 666 chemical reaction reaches completion were not affected by the initial momentum of the
 667 flow.

668 Appendix B. Range of chemical concentrations and buoyancy fluxes 669 used in the experiments

671 The range of conditions used in our fast-reaction experiments is given in tables 2
 672 and 3. It is seen that a number of different experiments were conducted, using plumes
 673 with: (i) different buoyancy fluxes and (ii) different concentrations of chemicals. In a
 674 first group of fast-reaction experiments (1-10 and 13-16 in tables 2 and 3), the source
 675 buoyancy flux B was fixed, while the ratio between the concentration of the chemical
 676 species in the plume and in the ambient fluid, C_b^0/C_a , was changed systematically. Since
 677 the chemical reactions used in these experiments did not affect B , the plume radius,
 678 speed and density were identical in this set of experiments. Tables 2 and 3 show that the
 679 critical stoichiometric dilution D_s ranged between 15 and 129 as a result of the different
 680 concentrations of chemical species used in the experiments (see equation 5.12); this in
 681 turn led to the stoichiometric length scale L_s varying between 10 and 38 cm in different

experiments (see equation 5.13). As discussed in section 5.5, owing to incomplete mixing of the fluid in the plume, the distance from the source at which the fast reaction reached completion was up to 1.6-1.8 times larger than L_s in our experiments (see figure 11b), leading to $z_r + z_0 \approx 60 - 65$ cm. The investigation of the impact of a wider range of chemical concentrations would have been difficult in the laboratory. Lower concentrations of reactants in the plume fluid would have resulted in $D_s < 10 - 15$ and $L_s < 10$ cm (see table 2): in this case, the supplied chemical species would have been neutralised at small distances from the nozzle, where the plume flow may be somehow affected by the initial momentum and source conditions (see appendix A). Higher concentrations of supplied reactant would result in $D_s > 130 - 150$, and thus the reaction would have reached completion at large distances from the source, which are incompatible with the vertical dimension of the experimental tank.

Equations 5.21 and 5.26 indicate that there is one key parameter in the model, z_{crit} , which varies as a function of the buoyancy flux, and is not affected by the concentration of chemical species in the plume. Hence, two additional experiments (11 and 12 in table 2) were performed using the same chemical properties as in experiment 4, but different buoyancy fluxes. In order to obtain different values of B , either different densities of the plume fluid, g'_0 , or different volumetric flow rates, Q_0 , could have been used at the plume source. For the source conditions of experiments 11 and 12 to be as close as possible to those of the other experiments, we chose to only let g'_0 vary, and kept the source volume flux Q_0 fixed (see table 2). This resulted in Re_0 , Γ_0 and L_{M_0} being the same across the different experiments. In order to increase the source density of the plume fluid, inert NaCl was added to the fluid as discussed in section 3.1. The ratio between the largest to the smallest values of g'_0 that we could achieve was 4. Since $z_{\text{crit}} \sim B^{-1/2}$ (see equations 5.21 and 5.26), this resulted in the critical distance z_{crit} varying by a factor 2 among the different experiments. The impacts of such a variation on the profile of concentration of chemical species in the plume were large enough that they could be measured using our experimental procedure.

REFERENCES

- ATKINS, P. W. 1978 *Physical Chemistry*. Oxford University Press.
- BATCHELOR, G. K. 1959 Small-scale variation of convected quantities like temperature in turbulent fluid. *J. Fluid Mech.* **5**, 113–133.
- BOWER, D. J., CAULFIELD, C. P., FITZGERALD, S. D. & WOODS, A. W. 2008 Transient ventilation dynamics following a change in strength of a point source of heat. *J. Fluid Mech.* **614**, 15–37.
- CAMPBELL, A. N. & CARDOSO, S. S. 2010 Turbulent plumes with internal generation of buoyancy by chemical reaction. *J. Fluid Mech.* **655**, 122–151.
- CARDOSO, S. S. & MCHUGH, S. T. 2010 Turbulent plumes with heterogeneous chemical reaction on the surface of small buoyant droplets. *J. Fluid Mech.* **642**, 49–77.
- CAULFIELD, C. P. & WOODS, A. W. 1995 Plumes with non-monotonic mixing behaviour. *Geophys. Astrophys. Fluid Dyn.* **79**, 173–199.
- CONROY, D. T. & LLEWELLYN SMITH, S. G. 2008 Endothermic and exothermic chemically reacting plumes. *J. Fluid Mech.* **612**, 291–310.
- DOMINGOS, M. G. & CARDOSO, S. S. 2013 Turbulent two-phase plumes with bubble-size reduction owing to dissolution or chemical reaction. *J. Fluid Mech.* **716**, 120–136.
- DOMINGOS, M. G. & CARDOSO, S. S. 2015 Turbulent thermals with chemical reaction. *J. Fluid Mech.* **784**, 5–29.
- FOX, R. O. 2003 *Computational Models for Turbulent Reacting Flows*. Cambridge University Press.

- 730 GEORGE, W. K., ALPERT, R. L. & TAMANINI, F. 1977 Turbulence measurements in an
731 axisymmetric buoyant plume. *Int. J. Heat Mass Transfer* **20**, 1145–1154.
- 732 HOUSECROFT, C. E. & CONSTABLE, E. C. 2002 *Chemistry, Equilibria*. Prentice Hall, Essex.
- 733 HUNT, G. R. & KAYE, N. G. 2001 Virtual origin correction for lazy turbulent plumes. *J. Fluid*
734 *Mech.* **435**, 377–396.
- 735 HUNT, G. R. & VAN DEN BREMER, T. S. 2011 Classical plume theory: 1937–2010 and beyond.
736 *IMA Journal of Applied Mathematics* **76**, 424–448.
- 737 KOMORI, S. & UEDA, H. 1984 Turbulent effects on the chemical reaction for a jet in a
738 nonturbulent stream and for a plume in a grid-generated turbulence. *Phys. Fluids* **27**,
739 77–86.
- 740 KUNDU, P. K., COHEN, I. M. & DOWLING, D. R. 2015 *Fluid Mechanics*. Amsterdam Academic
741 Press.
- 742 LEAIST, D. G. 1988 The effects of aggregation, counterion binding, and added nacl on diffusion
743 of aqueous methylene blue. *Canadian Journal of Chemistry* **66(9)**, 2452–2457.
- 744 LINDEN, P. F., LANE-SERFF, G. F. & SMEED, D. A. 1990 Emptying filling boxes: the fluid
745 mechanics of natural ventilation. *J. Fluid Mech.* **212**, 309–335.
- 746 LUPTON, J. E., DELANEY, J. R., JOHNSON, H. P. & TIVEY, M. K. 1985 Entrainment and
747 vertical transport of deep-ocean water by buoyant hydrothermal plumes. *Nature* **316**,
748 621–623.
- 749 MINGOTTI, N. & WOODS, A. W. 2015 On the transport of heavy particles through a downward
750 displacement-ventilated space. *J. Fluid Mech.* **774**, 192–223.
- 751 MINGOTTI, N. & WOODS, A. W. 2016 On turbulent particle fountains. *J. Fluid Mech.* **793**,
752 R1–1–R1–12.
- 753 MORTON, B. R., TAYLOR, G. & TURNER, J. S. 1956 Turbulent gravitational convection from
754 maintained and instantaneous sources. *Proc. R. Soc. Lond. A* **234**, 1–23.
- 755 MOWRY, S. & OGREN, P. J. 1999 Kinetics of methylene blue reduction by ascorbic acid. *J.*
756 *Chem. Educ.* **76**, 970–973.
- 757 NOULTY, R. A. & LEAIST, D. G. 1984 Activity coefficients and diffusion coefficients of dilute
758 aqueous solutions of lithium, sodium, and potassium hydroxides. *Journal of Solution*
759 *Chemistry* **13**, 767–778.
- 760 PAPANICOLAOU, P. N. & LIST, E. J. 1988 Investigations of round vertical turbulent buoyant jets.
761 *J. Fluid Mech.* **195**, 341–391.
- 762 PERRY, R. H. & GREEN, D. W. 2008 *Perry's Chemical Engineers' Handbook, Eighth Edition*.
763 McGraw-Hill.
- 764 POPE, S. B. 2000 *Turbulent flows*. Cambridge University Press.
- 765 SHAMIM, M. & BAKI, S. M. A. 1980 Diffusion measurements in aqueous l-ascorbic acid solutions.
766 *Aust. J. Chem.* **33**, 1857–1861.
- 767 SNEHALATHA, T., RAJANNA, K. C. & SAIPRAKASH, P. K. 1997 Methylene blue - ascorbic acid,
768 an undergraduate experiment in kinetics. *J. Chem. Educ.* **74**, 228–233.
- 769 SOMEYA, S., YOSHIDA, S., TABATA, T. & OKAMOTO, K. 2009 The effect of chemical reaction
770 on the mixing flow between aqueous solutions of acetic acid and ammonia. *International*
771 *Journal of Heat and Mass Transfer* **52**, 4236–4243.
- 772 SPARKS, R. S. J., BURSIK, M. I., CAREY, S. N., GILBERT, J. S., GLAZE, L. S., SIGURDSSON,
773 H. & WOODS, A. W. 1997 *Volcanic plumes*. Wiley.
- 774 ULPRE, H., EAMES, I. & GREIG, A. 2013 Turbulent acidic jets and plumes injected into an
775 alkaline environment. *J. Fluid Mech.* **734**, 253–274.
- 776 VITAGLIANO, V. & LYONS, P. A. 1956 Diffusion in aqueous acetic acid solutions. *J. Am. Chem.*
777 *Soc.* **78(18)**, 4538–4542.
- 778 WITTKE, G. 1983 Reactions of phenolphthalein at various ph values. *J. Chem. Educ.* **60**, 239–
779 240.
- 780 WOODS, A. W. 2010 Turbulent plumes in nature. *Annu. Rev. Fluid Mech.* **42**, 391–412.
- 781 WOODS, A. W. & CAULFIELD, C. P. 1992 A laboratory study of explosive volcanic eruptions.
782 *Journal of Geophysical Research* **97**, 6699–6712.
- 783 YE, H. & WILLS, G. B. 1971 Diffusion coefficient of aqueous nitric acid at 25°C as function of
784 concentration from 0.1 to 1.0 M. *Journal of Chemical and Engineering Data* **16**, 76–77.